



Can near-surface velocity structure be improved via dispersion analysis of conventional reflection data?

Shaun Strong *

Velseis Pty Ltd, University of Qld
sstrong@velseis.com

Steve Hearn

Velseis Pty Ltd, University of Qld
sheveh@velseis.com

SUMMARY

A recent ultra-shallow 3C survey provides an attractive dataset for evaluation of surface-wave dispersion analysis, for improving knowledge of the near-surface. The primary motivation is for S-wave reflection processing, but with potential for P-wave static control. Finite-difference modelling and real data analysis suggests maximum-offset should be set at several times the investigation depth. This study suggests the geophone interval should be less than 10m, and single phones are preferred. An inverted near-surface S-wave section provides structural information complementary to that available from P-wave refraction.

Key words: S-wave reflection, Dispersion, MASW

INTRODUCTION

Statics provide a major source of error in many conventional onshore seismic programs. The problem of accurately defining near-surface velocity structure is particularly challenging in the case of converted-wave and pure S-wave reflection, where serious static errors can render imagery unusable. In ultra-shallow S-wave surveys, statics may not be relevant since the reflection is actually targeting the near-surface variations. In this case, however, knowledge of near-surface S velocities is still very important for stacking. Prompted mainly by such requirements for S-wave work, we have examined whether surface-wave dispersion can contribute to an understanding of the near surface S-wave structure. However, as clarified below, the investigation also has relevance to conventional P-wave exploration.

An attractive dataset for this evaluation emerged from a recent 2D seismic survey aimed at imaging structures in shallow exploration targets, and determining if these structures extend upwards into the weathering layer. The survey consisted of a single 2D seismic line acquired with 4 separate configurations. Phase 1 was a standard high-resolution P-wave survey (28Hz geophones at a spacing of 4m) with a Vibroseis source. This focused on the main exploration targets (depths 30-200m).

NUMERICAL MODELLING OF SURFACE-WAVE DISPERSION

Real dispersion data can be complex and difficult to interpret. Numerical models provide a valuable starting point for understanding the concept, and evaluating the feasibility of achieving dispersion interpretations in real situations. Figure 1 shows a simplified weathering model, with near-surface

Phase 2 was a trial to determine which methods provide the best image of the ultra-shallow environment (0-50m). This included a very high resolution P-wave survey (28Hz geophones at a spacing of 1m) and a multicomponent survey (10Hz 3C geophones at a spacing of 3m) which included both P-wave and SH-wave sources. For an in-depth analysis of the P-wave data refer to Meulenbroek (2015). The majority of the S-wave processing was relatively straight forward. However, the velocity analysis proved to be quite difficult. In particular, it was apparent that standard velocity analysis was introducing erroneous structures due to the combination of low signal-to-noise ratio, low velocities, shallow reflectors and coherent noise swamping the near offsets. An alternative source of S-wave velocity information was needed.

The dispersion characteristics of ground roll are dominated by S-wave structure (Dorman and Ewing, 1962). The P-wave sources used in our survey generated strong ground roll, and this provided the motivation for this study. The particular ultra-shallow dataset being examined has the advantage of providing a best-case scenario in respect of geophone spacing. However, the data also allow conclusions to be drawn regarding seismic surveys at high-resolution and petroleum scales.

The study of surface-wave dispersion has a long history in earthquake seismology (e.g. Macelwane, 1923). In the applied context, the MASW technique was evolved in the late 90s (eg. Park et. al., 1999). It has had a broad range of applications including direct S-wave velocity measurement and S-wave static correction (eg. Roy et. al., 2010). Dal Moro et. al. (2005) compared the S-wave velocity profile generated from standard reflection analysis with another generated from MASW.

In brief, the standard MASW technique requires that a shot record be transformed into phase-velocity versus frequency (or period) space. For this investigation an FK-based algorithm has been used. The dispersion curves are picked from the velocity-frequency display, and in theory can then be inverted to give a 1D geological model.

parameters based on a particular survey, but broadly representative of many land acquisition cases. We have used finite-difference code (e.g. Strong and Hearn, 2008) to simulate vertical and inline component shot records, and then have performed dispersion analysis on the shot records (using an FK approach).

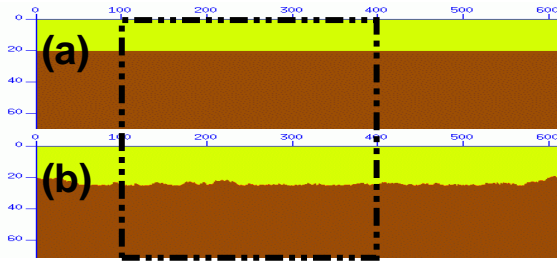


Figure 1: Geological Models used by elastic finite-difference algorithm to produce shot records. (a) 20m deep weathering layer (yellow) with $V_p=800\text{m/s}$ $V_s=400\text{m/s}$ overlaying a basement of $V_p=2500\text{m/s}$ $V_s=1250\text{m/s}$. (b) weathering depth is varied to produce a more realistic response. The black rectangle represents the offset range of the shot records of interest (ie $\text{maxoffset}=300\text{m}$).

Figures 2 (a) and (b) show the derived vertical and inline dispersion curves (up to 75 Hz) corresponding to the regular model in Figure 1(a). On the vertical data, the fundamental mode (Mode 0) is well defined above about 10 Hz. The lower-frequency attenuation results partly from the wavelet used in the modelling, and simulates what can be expected from use of 10 Hz geophones. Several higher modes are visible, and these are generally much stronger on the inline component. For comparison, Figures 2(c) and (d) show a dispersion analysis from the more realistic irregular-bedrock model in Figure 1(b). There is considerable weakening and distortion in the higher modes. The fundamental mode is relatively unaffected.

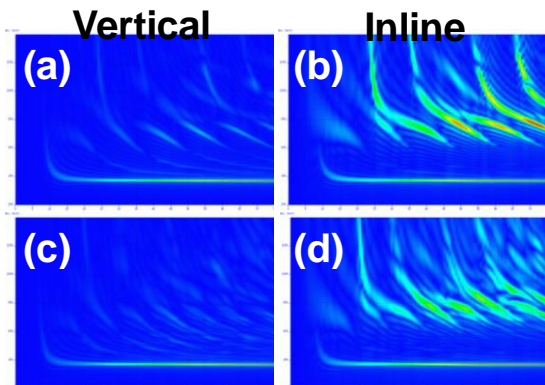


Figure 2: Dispersion response of the vertical and inline records derived from the constant (a & b) and variable (c & d) depth models in Figure 1. The dispersion plots have ranges 200-1400m/s (vertical axis) and 0-75 Hz (horizontal axis)

Dispersion interpretation assumes a laterally homogenous near surface. Failure of this assumption is evident in the simple example of lateral distortion seen in Figure 2. For this reason, there is an argument that dispersion analysis should be performed over a restricted lateral range. Figure 3 (a) and (b) shows the dispersion analyses for the constant-depth model of Figure 1(a), when the maximum offset has been reduced from 300m to 100m. Figure 3 (c) and (d) shows the same reduced-offset analysis for the variable-depth model of Figure 1(b). Comparison with Figure 2 illustrates that while offset-restriction is desirable from the point of view of lateral consistency, it has the undesirable effect of a significant loss of resolution.

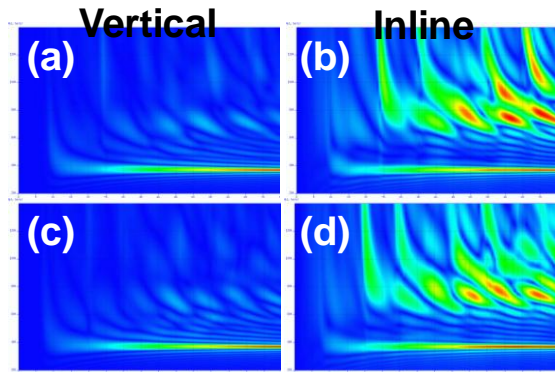


Figure 3: Dispersion response for the limited offset records ($\text{maxoffset}=100\text{m}$) corresponding to the constant (a & b) and variable (c & d) depth models.

Next we examine the influence of geophone interval. The model shot records analysed to this point were constructed with a best-case geophone interval of 1m. For economic reasons such a fine interval would only normally be used in ultra-shallow surveys. In Figure 4 (a) (b) (c) we simulate the dispersion analyses derived for single-geophones spaced at 4m, 8m, and 16m respectively. To concentrate on the influence of geophone spacing, we have reverted to the simpler homogenous weathering model, and include an offset range up to 300m. A geophone spacing of 4m gives a result almost equivalent to the ideal 1m result (at least within the frequency range being considered here). However when the spacing is increased to 8m, we see a very strong aliased event interfering with the highest modes on both the vertical and inline components. When the spacing is further increased to 16m, the aliased events extend even further into the analysis space, such that all but the fundamental mode are subject to interference. Finally, in Figure 4(d) we show the analysis corresponding to a 16m group interval, but with a group of 16 phones at 1m, rather than a single geophone. This is representative of parameters common on many petroleum-scale 2D surveys. The use of a 16m group seems to provide improved amplitude definition, but even greater aliasing distortion than in the case of single-phones at 16m.

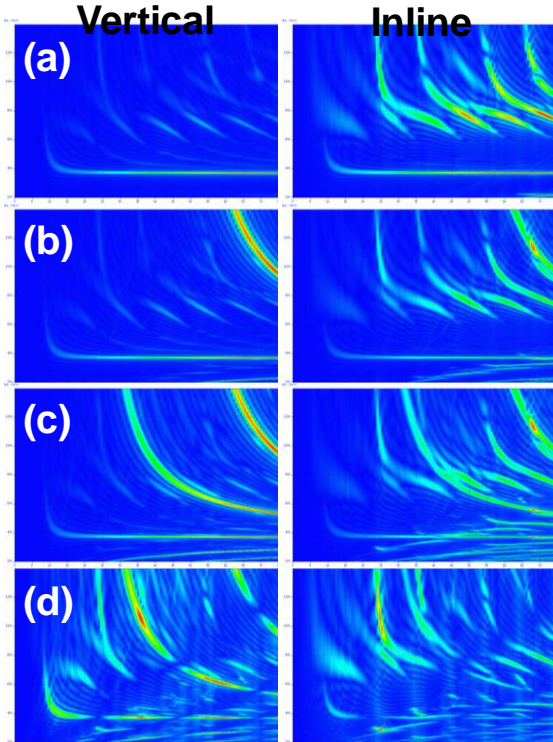


Figure 4: Effect of geophone spacing on dispersion response. Images (a), (b), and (c) have been created by decimating the shot records to produce geophone spacings of 4m, 8m and 16m respectively. Image (d) has a 16m group interval with geophone spacings of 1m.

To this point we have focussed on the appearance of the computed dispersion curves as various model and recording parameters are varied. Finally we consider the problem of correctly identifying various dispersion modes on analysed data. In Figure 5 we return to the best-case scenario of a homogenous model, a maximum offset of 300m, and geophone interval of 1m. The red dashes show auto-picked modes derived from the analysis. Superimposed also are the true dispersion modes derived using the standard Thomson-Haskell approach (Haskell, 1953). The main observation is that even with best-case data analysis, it is very easy to misinterpret modes on such analyses. For example, note the difficulties around the low-frequency ‘kissing point’ between Modes 0 and 1. Note also the danger of the interpretation jumping from one mode to another (e.g. Modes 2,3,4,5 on vertical component).

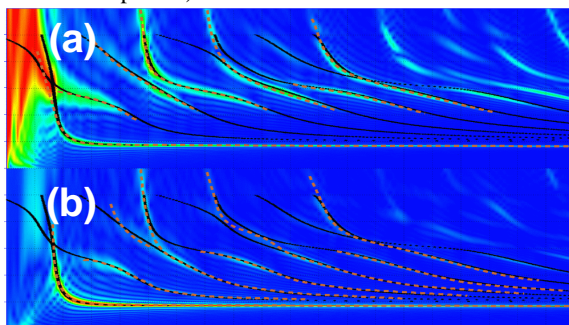


Figure 5: Comparison of picked dispersion modes (red dashed) with theoretical modes (black) generated by the Thomson-Haskell approach. (a) Inline dispersion plot, (b) Vertical dispersion plot.

REAL DATA EVALUATION

Figure 6 shows vertical and inline components of a representative shot from the ultra-shallow 3C survey. The source was a manually operated vertical impactor (*Bigfoot*, see Meulenbroek, 2015), and 10-Hz 3C geophones were deployed at an interval of 3m. Surface waves are well developed. The dispersion analysis was restricted to an 80m offset zone (marked in red) in order to reduce the effects of lateral variation. Figure 7 shows the extracted dispersion curves obtained via the FK approach. The general appearance in terms of resolution is similar to that seen on the offset-limited numerical data.

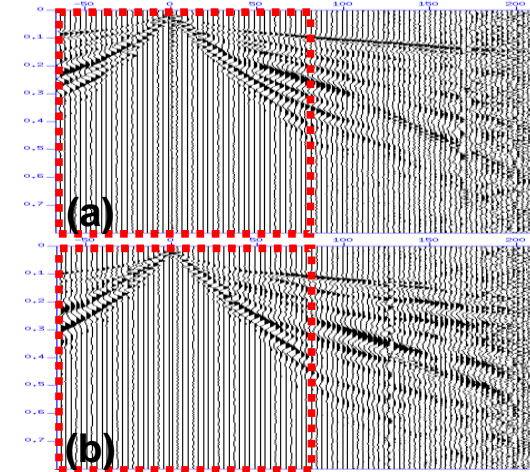


Figure 6: Vertical (a) and inline (b) records corresponding to source point 121. The red box indicates the data included for dispersion analysis and corresponds to a max absolute offset of 80m. Note that there are strong surface wave events within these offsets.

Mode 0 is well defined on both the vertical and inline analyses, and Mode 1 appears to exist on the vertical component. Recall that on the model data, higher modes appeared much more strongly on the inline component. This effect is not obvious on this real dataset. It was noted on model data that these higher modes were more susceptible to the effects of lateral inhomogeneity, offset limiting and increasing geophone interval. This may contribute to their poor definition on the real data.

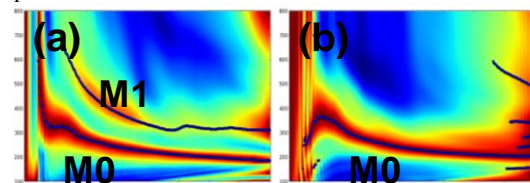


Figure 7: The vertical (a) and inline (b) dispersion response corresponding to the records in Figure 6. The blue points are automatically picked based on local maxima analysis and threshold restriction. These generally correspond to dispersion curves although there are some erroneous picks

As in the case of the model data, it is of interest to examine how the definition of dispersion curves is affected when the geophone spacing is increased. In Figures 8(a)-(d) we show the dispersion curves resulting from decimation of the shot records from the original 3m to 9m and 15m respectively.

As seen with the model data, increased geophone intervals lead to increasingly severe aliasing distortion. However, provided that the positioning of these aliased curves are understood, the 9m simulation (Figures 8(a),(b)), appears to provide good definition of Mode 0 on both components, and Mode 1 on the vertical. When the geophone interval is increased further to 15m (Figure 8(c),(d)) there is still evidence of Modes 0 and 1, but they suffer more severe distortion from aliased noise. Figure 8(e),(f) simulates a recording with a 15m group interval, but using 5 geophones at 3m, rather than a single geophone. As with the model data, the use of a group seems to provide improved amplitude definition, but at the cost of increased aliasing distortion. In summary, these tests would appear to mandate a geophone interval of less than 10m for this dataset.

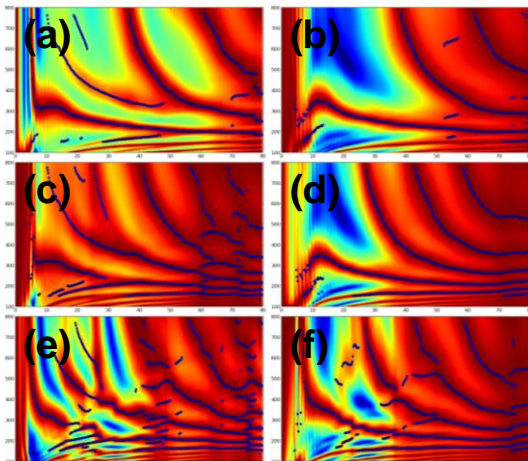


Figure 8: Effect of geophone spacing on dispersion response. Images correspond to vertical (a,c,e) and inline (b,d,f) dispersion responses. The records in Figure 6 have been decimated to give dispersion curves for geophone spacings of 9m (a,b) and 15m (c,d). Images (e,f) have a 15m group interval with geophone spacings of 3m.

INVERSION AND INTERPRETATION

We have performed surface-wave inversion using the standard CPS-SURF96 package (Hermann and Ammon, 2002). Figures 9 (a) and (b) summarise the velocity model (left) and corresponding dispersion curve fit corresponding to the representative dispersion curves (vertical component) in Figure 7. Inversions have been run incorporating just Mode 0 (Figure 9(a)) and both Modes 0 and 1 (Figure 9(b)). The results for this shot are quite representative of other shots. When just Mode 0 is used, a generally good fit can be achieved. When Mode 1 is also included, the overall fit is arguably reduced. The velocity models obtained with the two approaches exhibit broadly similar features. Our experience suggests that inclusion of Mode 1 is useful provided it can be confidently identified.

We have applied the process described here to 200 shots, yielding a 600m S-wave inversion section. Figure 10(a) shows the inversion section based on Mode 0 alone, while Figure 10 (b) shows the inversion based on both Modes 0 and 1. The shallowest low-velocity layer agrees well with P-wave refraction data (Meulenbroek, 2015) and is interpreted as a soil layer. The deepest transition (around 20-25m) is also in general agreement with the base of weathering from the corresponding P-wave refraction and reflection analysis. The S-wave velocity inversion occurring around 10-15m appears

quite robust in our tests. This inversion would not be detectable on the P-wave data.

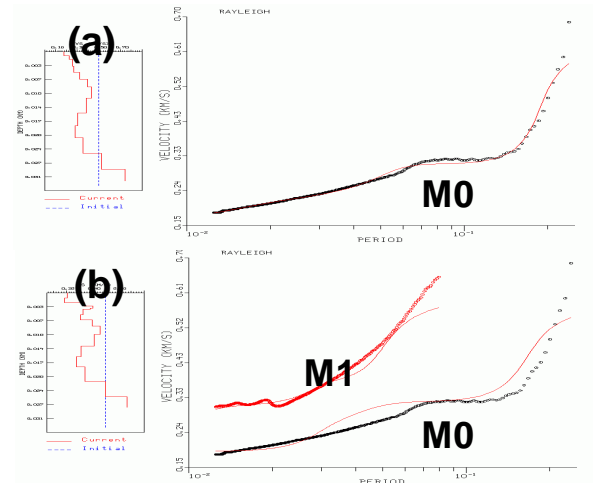


Figure 9: Inversion of the edited dispersion picks (Right derived from Figure 7) to generate a geological model (Left). (a) Including only Mode 0, (b) including Modes 0 and 1. S-wave velocities range from 200-800m/s.

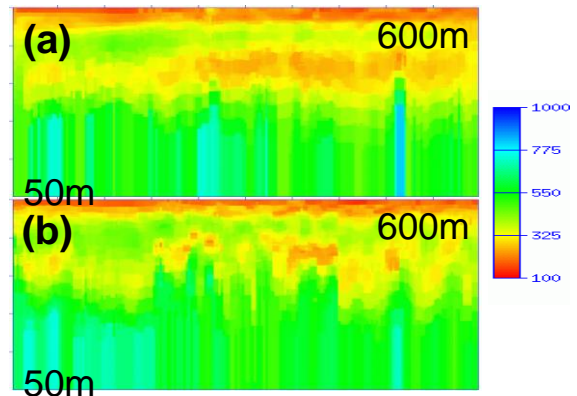


Figure 10: Inverted S-Wave velocity section generated from 200 source locations (600m). A 5-station horizontal median filter has been applied to remove anomalous results.

CONCLUSIONS

Numerical modelling provides a powerful tool for understanding surface-wave dispersion resulting from the weathered zone, and evaluating the influence of earth-model parameters, acquisition geometries, and analysis algorithms. Model dispersion curves exhibit much stronger higher-modes on the inline component, with potential for improving control of inversions. However, this was not replicated on the real-data tests. Offset limiting is valid from the viewpoint of reducing the effect of lateral variations, but compromises resolution. Our experience suggests that it is appropriate to set the maximum offset to several times the maximum depth being investigated. Aliasing distortion results from increasing geophone intervals. The weathering situation in the region of our work is broadly typical of many onshore situations. This case-study suggests that a geophone interval of less than 10m is desirable, and that single-geophones are preferable to groups.

The evaluation done here was prompted by availability of an ultra-shallow survey, with finely spaced 3C geophones.

Nevertheless, the observations are relevant to petroleum and coal scale surveys, where good definition of the near surface quality. The trials described here suggest that dispersion analysis may be feasible using standard production- scale vertical-component data. The derived surficial S-wave models could provide useful controls for P-wave statics models.

ACKNOWLEDGEMENTS

Parts of the processing used Seismic Unix from Colorado School of Mines. Many thanks to Velseis staff who assisted in this experimental field project.

REFERENCES

Dal Moro G.M., Pipan M., Forte E., Gabrielli P., Sukan M., Forlin E., Finetti I., 2005, Shear-wave Profiling via SH reflection analysis and rayleigh wave inversion. SEG Abstract p1049-1052.

Dorman J., Ewing M., 1962, Numerical inversion of seismic surface wave dispersion and crustal-mantle structure in the New York-Pennsylvania area. Journal of Geophysical Research, V67(13) p5227-5241.

Haskell, N.A., 1953, The dispersion of surface waves on multilayered media, Bulletin Seismological Society America, V43, 17-34.

can assist greatly in static solutions and hence overall image

Herrmann, R.B., Ammon, C.J., 2004, Surface waves, receiver functions and crustal structure. Computer Programs in Seismology, Version 3.30 [Electronic]. Saint Louis Univ, St. Louis, Mo. Available at <http://www.eas.slu.edu/People/RBHerrmann/CPS330.html>.

Meulenbroek, A., 2015, Integrated reflection and refraction processing of an ultra-shallow seismic survey. Extended Abstract, ASEG 24th International Geophysical Conference and Exhibition.

Macelwane, J.B., 1923, A study of the relation between the periods of elastic waves and the distance travelled by them, based upon the seismographic records of the California earthquake, January 31, 1922. Bulletin Seismological Society America, V13, 13-69.

Park C.B., Miller R.D., Xia J., 1999, Multichannel analysis of surface waves. Geophysics, V64(3), p800-808.

Roy S., Stewart R.R., Dulaijan K.A., 2010, S-wave velocity and statics from ground-roll inversion. The Leading Edge, p1250-1257

Strong, S. and Hearn, S., 2008, Multi-component seismic-resolution analysis using finite-difference acquisition modelling. Exploration Geophysics 39, 189–197.